On the interactions between carbohydrates and immune cells

Steuten, K.

Chapter 6

Summary and future prospects

6.1 Summary

The work presented in this thesis established two quantitative methods for measuring carbohydrate–immune cell interactions in complex cellular and *in vivo* environments. The first method considers the Glyco-PAINT-APP for which the development is described in **Chapter 2** and the functional correlation studies in **Chapters 3** and **4**. The second method is a single-cell glucose and glutamine uptake assay that is developed in **Chapter 5** and was applied to resolve the competition for these nutrients between cancer and immune cells in the tumor-microenvironment.

6.2 Quantitative kinetics using PAINT microscopy

The dawn of single-molecule localization microscopy has inspired several technological advances that resulted in new imaging methods.[1] PAINT-based methods uniquely allow for the use of physiological ligands for imaging and thereby also enable deriving kinetic parameters of the receptor-ligand pair. The Glyco-PAINT method, originally described by Riera *et al*.[2], is a super-resolution pointillism-based method where the inherently weak association between glycan ligands and their lectin receptors on cells is used to generate sparse blinking events that can, after recording over time, be reconstructed into tracks representing a single-molecule binding event on a live cell. **Chapter 2** describes the further development of the Glyco-PAINT technology and an associated automated processing pipeline such that the technique is compatible with cells on which binding events are not homogeneously distributed across the cell membrane such as primary immune cells. This was achieved via a subcellular segmentation approach that enabled automated, unbiased and high-throughput analysis of Glyco-PAINT recordings.

In future, this methodology could be used to quantify the kinetic parameters of any other receptor-ligand interaction of interest. For example, a technology using the inverse receptor-ligand pair of Glyco-PAINT has been demonstrated by Tholen *et al*. Here, fluorophore-labeled plant lectins were used to ”glycotype” the abundance, affinity and mobility of the cell surface glycocalyx of leukemia cell lines.[3] To streamline new applications of the technology into other receptor–ligand pairs, some considerations are listed below that may assist selection of fruitful research directions.

- **Biology is leading.** PAINT studies should be critically evaluated at the moment of conception for their usefulness. Does the quantification of the interaction kinetics between a new receptor–ligand pair really contribute to our understanding of a relevant biological phenomenon? For instance, quantifying the kinetics of an interaction that is already well-characterized, non-regulatory, or biologically inert under physiological conditions offers limited conceptual advance, even if technically feasible.

- **Affinity range.** The dissociation constant (K_D) of the interaction should be within a certain range. Too strong interactions would make it difficult to observe single-molecule events or may result in fluorophore bleaching before unbinding whereas too weak interactions would result in a too low event rate. A suggested rule of thumb for the K_D is in the 100 nM - 10 μM range.[4,5] When available, K_D values derived from immobilized receptor SPR studies may provide a good starting point. Ideally, on-cell kinetics such as those derived from flow cytometry assays may provide more accurate insight into the actual interaction on live cells.

- **Fluorophore.** The choice for a fluorophore for PAINT imaging is subject to some considerations. Generally, fluorophores with high brightness and a long photostability are optimal. Two important photophysical properties to consider are quantum yield, which is defined as the amount of absorbed photons that are converted into emitted photons and extinction coefficient, which is a measure of how many photons a fluorophore can absorb at a given wavelength. The product of these two parameters is defined as fluorophore brightness.[6] Photostability is defined as the fraction of fluorophore molecules that survive a certain illumination period. Practically, this implies that most often yellow, red or NIR-absorbing dyes with high photostability are ideal for PAINT imaging. The dyes ATTO532, ATTO643, sCy5 and ATTO655 have given good results in our and others' hands. A table with some commonly used fluorophores for superresolution microscopy and their properties is reported by Dempsey *et al*.[7]

- **Ligand.** In most PAINT imaging systems the ligand is modified with a fluorophore. To draw conclusions about single-molecule behavior of the interaction, it is critical that there is a single fluorophore attached per ligand. This is evident and controllable in the case of fully synthetic ligands such as for the carbohydrates in **Chapters 3** and **4**. When using protein ligands in combination with amine- or thiol-reactive chemistries the degree of labeling typically is more difficult to control which can lead to problematic data interpretation as discussed in Tholen *et al*.[3] Additionally, receptor-accessibility by the ligand should be considered when imaging adherent cells. Tightly adherent cells to the glass surface may prevent the use of higher molecular weight ligands such as proteins or protein complexes (e.g. MHC). Strategies that involve capturing of suspension cells with antibodies that are attached to the coverglass surface via linkers with tunable length may accommodate larger PAINT-ligands while keeping the cells in place.[3]

- **Receptor.** For initial testing of a new receptor–ligand pair a good cellular model system that is expressing the receptor of interest is extremely helpful. Equally important is a negative control system that lacks the receptor of interest. Ge-

netic overexpression cell lines may provide a good option for this but the expression dynamics, post-translational modifications, and nanoscale clustering may not strictly mimic the native biological situation. When interested in profiling endogenous receptors that are expressed on any cell type (e.g. galectins or mannose-6-phosphate receptors) overexpression or knock-out cells may technically not be feasible and thus one can resort to blocking antibodies or competition with dark ligands to set background levels. Cells of primary origin can be considered as model system but should ideally be studied together with genetic knock-outs to avoid difficulties with data interpretation arising from non-receptor mediated binding or binding to redundant receptors. Future work would benefit from less complex, non-cellular, benchmarking systems that can establish ground-truth binding using receptors immobilized on DNA-origami scaffolds analogously to the initial DNA-PAINT work.[8] Binding parameters established as such may aid in disentangling the complex binding profiles that are observed using Glyco-PAINT on live cells.

6.2.1 Statistical testing and pseudoreplication

The subsectioning method described in **Chapter 2** introduces a change in the unit of observation of Glyco-PAINT microscopy recordings. Instead of analyzing the entire basal membrane of a cell as a single unit, squared subregions of fixed size are sampled and analyzed individually. This strategy improves the spatial resolution for estimating subcellular binding kinetics and was deliberately chosen to capture the microheterogeneity that is characteristic for lectin dynamics on primary myeloid cells.

At the same time, this approach results in a substantial increase in the number of data points per recording that were previously considered single measurements. When all squares are treated as independent observations in a conventional F-test (such as ANOVA) statistical framework, this may challenge one of the core assumptions of the F-test, namely that all observations are statistically independent.[9] Adjacent squares originating from the same recording, or even from neighboring cells cultured within the same microscopy well, are likely to share experimental context, such as ligand availability, illumination conditions, or cellular state, which could introduce some degree of dependence between measurements. This phenomenon is known as *pseudoreplication* and is subject to debate in literature.[10,11]

Importantly, however, the extent of this dependence is not known *a priori*. Primary cells are highly heterogeneous, and Glyco-PAINT measurements often reveal strong spatial variability in receptor density and binding kinetics even within a single cell. It is therefore just as plausible that individual squares capture genuinely distinct kinetic behavior, rather than redundant measurements of the same underlying process. This microheterogeneity is, in fact, one of the main motivations for adopting a square-based subsampling strategy in the first place.

The potential issue of pseudoreplication is well recognized in other fields, such as longitudinal clinical studies or behavioral animal experiments, where repeated measurements from the same subject or shared animal housing conditions can lead to dependent data structures.[11] In the context of Glyco-PAINT, square-level analysis represents a trade-off between increasing spatial and statistical resolution on the one hand, and the risk of over-weighting correlated observations on the other. For this reason, alternative statistical approaches such as linear mixed-effects models that explicitly account for the nested structure of the data are explored in this section.

Below, the Glyco-PAINT binding data of sialyllactose probes to polarizing macrophages presented in **Chapter 4** are reanalyzed using three exemplary statistical approaches (**Figure 6.1a–c**).

1. **Square-level ANOVA**

   In the first approach (**Figure 6.1a**), each square is treated as an independent observation. A one-way ANOVA is applied to compare the mean of a kinetic parameter Y (e.g. residence time τ) across adjuvant conditions A_i:

   $$Y_{ij} = \mu + \alpha_i + \varepsilon_{ij}, \quad \varepsilon_{ij} \sim \mathcal{N}(0, \sigma^2)$$

   where Y_{ij} denotes the value measured in square j under adjuvant condition i, μ is the global mean, α_i is the fixed effect of adjuvant i, and ε_{ij} is the residual error term. The notation $\varepsilon_{ij} \sim \mathcal{N}(0, \sigma^2)$ indicates that residuals are assumed to be normally distributed ($\mathcal{N}$) with mean 0 and variance σ^2, capturing random deviations from the group mean.

   From general statistical methods, the ANOVA F-statistic is defined as the variance between groups divided by the variance within groups.[12] The term variation refers to the sum of squared deviations of observations from their mean (MS) and is applied as follows:

   $$F = \frac{\text{MS}_{\text{between}}}{\text{MS}_{\text{within}}} = \frac{\frac{\sum_i n_i(\bar{Y}_i - \bar{Y})^2}{k-1}}{\frac{\sum_i \sum_j (Y_{ij} - \bar{Y}_i)^2}{N-k}}$$

   where n_i is the number of squares in group i, k is the number of adjuvant conditions, and $N = \sum_i n_i$ is the total number of observations. The numerator captures differences between group means, while the denominator captures variability within groups.

   Importantly, the number of squares N directly influences the denominator degrees of freedom $(N-k)$. As N increases, the estimate of within-group variance becomes more precise under the assumption of independence, and the standard error (SE) of group means decreases approximately as:

   $$\text{SE} \propto \frac{\sigma}{\sqrt{n_i}}.$$

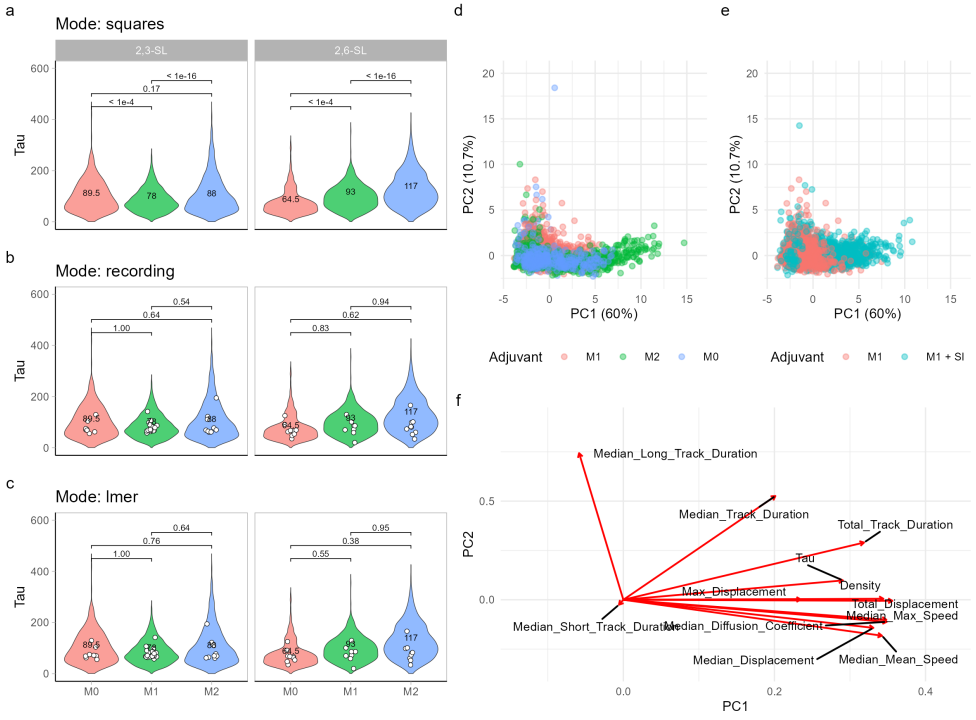

Figure 6.1: Comparison of statistical methods and dimensionality reduction for binding of monovalent sialyllactose probes to polarizing macrophages Violin distribution plots for the calculated τ per square across M0, M1 and M2 polarization states analyzed via three different statistical approaches. In (**a**) p-values are computed with a square-level ANOVA, in (**b**) a recording-level ANOVA and in (**c**) linear mixed-effects modeling was applied. (**d**) Dimensionality reduction using PCA of several kinetic parameters per square for 2,3-SL binding to M0, M1 and M2 macrophages. (**e**) PCA plot for 2,3-SL binding to M1 or M1 + SI treated (see **Chapter 4**) macrophages. (**f**) PCA loading plot for **d** and **e** identifying the features driving variance, where vector length and direction indicate the contribution of specific metrics (see methods for a full list of parameters) to the global variance. Significance annotations in (**a-c**) represent p-values adjusted for multiple comparisons. White points in **b** and **c** represent the recording means.

This leads to larger F-statistics and therefore smaller p-values, even when the absolute differences between group means remain unchanged.

After this analysis, pairwise comparisons are performed using Tukey's Honest Significant Difference (HSD) test, which controls for multiple testing by adjusting the significance threshold based on the number of group comparisons.

In the analysis in **Figure 6.1a**, this approach yields small p-values for most comparisons of τ across adjuvants, reflecting the large number of squares. However, if squares within a recording are not fully independent, the effective sample size is overestimated, which can lead to inflated F-statistics and artificially small p-

values (pseudoreplication).

2. **Recording-level ANOVA**

   In the second approach (**Figure 6.1b**), square-level measurements are first averaged within each recording, yielding one value per recording and adjuvant condition:

$$\bar{Y}_{ik} = \mu + \alpha_i + \varepsilon_{ik}, \quad \varepsilon_{ik} \sim \mathcal{N}(0, \sigma^2)$$

   where $\bar{Y}_{ik}$ is the mean kinetic parameter across all squares in recording k for adjuvant i.

   This aggregation reduces the effective sample size to the number of recordings and thereby limits the risk of pseudoreplication. The same ANOVA framework, residual calculation and Tukey HSD correction are then applied similarly as for the square-level ANOVA. This approach results in markedly larger p-values for all comparisons between adjuvants. Effects that appeared significant at the square level are now no longer statistically significant (**Figure 6.1b**). This suggests that some of the apparent effects in the square-level analysis may be inflated by repeated measurements within recordings, while averaging over recordings in the second approach can also reduce the signal, potentially obscuring true differences between experimental conditions.

3. **Linear mixed-effects modeling (LMM)**

   In the third approach (**Figure 6.1c**), the hierarchical structure of the data is modeled explicitly using a linear mixed-effects model:

$$Y_{ijk} = \mu + \alpha_i + b_k + \varepsilon_{ijk}, \quad \varepsilon_{ijk} \sim \mathcal{N}(0, \sigma^2)$$

   where Y_{ijk} denotes the value measured in square j of recording k under adjuvant condition i, μ is the global mean, α_i is the fixed effect of adjuvant, and b_k is a random intercept for recording k, assumed to be normally distributed as $b_k \sim \mathcal{N}(0, \sigma_b^2)$. The residual term ε_{ijk} captures square-level variability not explained by the model.

   In practice, this model corresponds to:

$$Y \sim \text{Adjuvant} + (1 \mid \text{Recording})$$

   p-values for adjuvant effects are obtained via pairwise contrasts of estimated marginal means (EMMs) computed using the `emmeans` framework.[13,14] In this implementation, the reported p-values correspond to pairwise contrasts between adjuvant conditions without additional multiple-testing correction beyond the contrast procedure itself.

Notably, the LMM yields p-values that are very similar to those obtained from the recording-level ANOVA, and no comparisons reach the significance threshold. This suggests that while accounting for within-recording correlation reduces apparent effects, other sources of dependency may exist, or that the current number of independent recordings (3 biological replicates with each 3 recordings, thus 9 in total) limits statistical power. For example, additional dependencies such as cell type, experiment date-level grouping, or spatial clustering could influence the data.

Taken together, these analyses indicate that square-level testing can potentially overstate significance, while both recording-level ANOVA and LMM provide more conservative and closely aligned results. The similarity between recording-level ANOVA and LMM outcomes implies that, in this dataset, mixed-effects modeling based on recording primarily revisits the dependency already addressed by averaging, rather than revealing new effects. Future studies would benefit from increased biological replication and from experimental designs that allow for explicit modeling of hierarchical or nested structures, potentially improving the ability to detect subtle effects. Ideally, *a priori* power calculations should be performed in consultation with expert biostatisticians in the field of high-throughput kinetic imaging analysis to identify the most appropriate statistical framework for this type of data.

6.2.2 Dimensionality reduction

In addition to univariate statistical testing, multi-dimensional data can be analyzed via principal component analysis (PCA) to evaluate the contributions of each dimension to the separation of individual datapoints or subclusters. PCA could be of use as an exploratory tool to assess which combinations of parameters could better separate adjuvant conditions (e.g. M0 vs M1 vs M2 or M1 vs M1 + SI) than individual metrics alone for the **2,3-SL** sialoside to macrophage binding dataset. To apply this analysis to Glyco-PAINT-APP square-based kinetic data, first a selection of suitable metrics (see methods for the selected parameters) was made that were each normalized within the entire dataset. The first principal component (PC1) accounted for 60% of the total variance and showed the strongest separation between adjuvant conditions for Siglec binding (**Figure 6.1d, e**) which indicates that certain parameters explain a very large part of the variance. Furthermore, there is a large overlap between squares across adjuvant conditions for both comparisons. Inspection of the loading vectors, which indicate how much each variable contributes to the PCs, further indicates that all kinetic parameters, except the Median Long Track Duration, dominate the loading of PC1 (**Figure 6.1f**) as visualized by the directions of the arrows. As indicated by the high loading of PC1, these parameters also explain the majority of the variance in the data. This, together with the absence of distinct separation between the adjuvant clusters,

implies a strong correlation among the measured variables of which many are derived from the same underlying binding trajectories.

As a consequence, PCA in this context primarily re-encodes correlated information rather than uncovering independent biological dimensions. While PCA provides a visual summary of variance structure for the binding data, it does not improve interpretability or statistical inference beyond the univariate analyses presented above. This limitation reflects both the correlated nature of the kinetic parameters and the relatively small number of independent biological units. Future analyses may benefit from reducing parameter redundancy prior to dimensionality reduction or from incorporating additional, fully orthogonal, measurements to the datasets such as receptor co-staining or cell surface marker co-staining as a means to provide more insight into the actual binding partners within inherently heterogeneous samples such as myeloid cells.

6.3 Correlations between glycan binding and immune cell functionality

6.3.1 MR-dependent cross-presentation

In **Chapter 3** binding of mannosylated SLPs was correlated to myeloid cell functions such as uptake capacity and antigen cross-presentation. The inverse correlation between SLP glycosylation and cross-presentation touches an historical controversy centered around the role of the MR in raising an adaptive immune response in mice.[15–18] Whereas these reports use whole protein antigen, data on the efficacy of mannosylated peptides containing the $Ovalbumin_{263\text{-}275}$ epitope is currently limited to a single report by Rauen *et al*.[19] Here, a beneficial effect of sugar attachment on T cell activation was reported which conflicts with our results. However, mannosides with different linkages and complexity were used in this work compared to those used here.

Future work might benefit from a reproduction study followed by exact side-by-side comparison of the SLPs from Rauen *et al.* with the SLPs from **Chapter 3** in Glyco-PAINT and cross-presentation assays. Additionally, vaccination studies with these SLPs in WT and $MR^{-/-}$ mice could shed light on their effectiveness in physiological settings. To further investigate the observed correlation between SLP residence time on the DC cell surface and cross-presentation several approaches could be employed. First, small mutations in the antigenic peptide with known effects on cross-presentation efficiency and MHC-I affinity could be studied (e.g. `EIINFEKL`, `SIIRFEKL`, `SIIGFEKL`) to test if the correlation is consistent for epitopes with reduced potency.[20] Additionally, completely different CD8 T cell antigens from cancer or viral sources decorated with similar glycosylation patterns could be evaluated to test if the correlations are dependent on the physicochemical parameters of the pep-

tide epitope.

6.3.2 Identifying Siglec binding partners

In **Chapter 4** the desialylation (and thus removal of *cis* ligands) on M1 macrophages by sialyltransferase inhibitor treatment resulted in enhanced binding by the *trans* ligands **2,3-SL** and **(2,3-SL)$_3$**. Interestingly, this effect was more pronounced for inhibitor treatment than for Sialidase treatment which in turn contrasted to the absolute amounts of residual sialic acid on the macrophage cell surface as determined by lectin staining.

This observation raises the question of which of the Siglecs is the responsible binding partner that enables this effect after unmasking. To further investigate the identity of this binding partner, expression levels of the individual Siglecs could be determined followed by differentiation of macrophages from knock-out mice that are genetically lacking the suspected Siglecs. Initial steps in this direction were undertaken by performing quantitative, LC-MS/MS whole cell proteomics. For this we used a suspension-trapping protocol that enables label-free quantification of the whole cell proteome. From this analysis, Siglec-1 (SN_MOUSE, Sialoadhesin), Siglec-2 (CD22_MOUSE) and Siglec-12 (SIG12_MOUSE, Siglec-E) were identified of which only Siglec-E showed significant upregulation in M1 macrophages (**Figure 6.2b, c**). Next to the relevant polarization markers (CD86_MOUSE for M1 and MRC1_MOUSE for M2) that were found to be specifically upregulated, also $\alpha 2,6$-Sialyltransferase (SIA7D_MOUSE or ST6GalNAc) showed increased expression in M1 macrophages (**Figure 6.2a**).

These results point at Siglec-E as a potential binding partner for sialoside binding on M1 macrophages. Together with upregulated sialyltransferase activity this might explain the observed increase in sialoside binding parameters after removal of *cis*-ligands by SI treatment. Glyco-PAINT studies using macrophages generated from Siglec-E$^{-/-}$ mice[21] could further confirm this hypothesis.

6.4 Selectivity and kinetics of 6-DAG

In **Chapter 5** the bioorthogonal glucose analog 6-deoxy-alkynyl-glucose (6-DAG) was identified. This molecule showed improved signal-to-noise ratios and selectivity over the previously reported bioorthogonal glucose probe 6AzGal[22] and could be multiplexed with a previously established bioorthogonal glutamine uptake assay to profile nutrient uptake in the mouse tumor micro-environment.

For the selectivity of 6-DAG there was still a portion of the uptake signal in *ex vivo* immune cells that remained insensitive to glucose-competition. To further elucidate the cellular or physicochemical mechanisms that contribute to this transporter-independent uptake, several strategies could be used. First, transgenic animals where

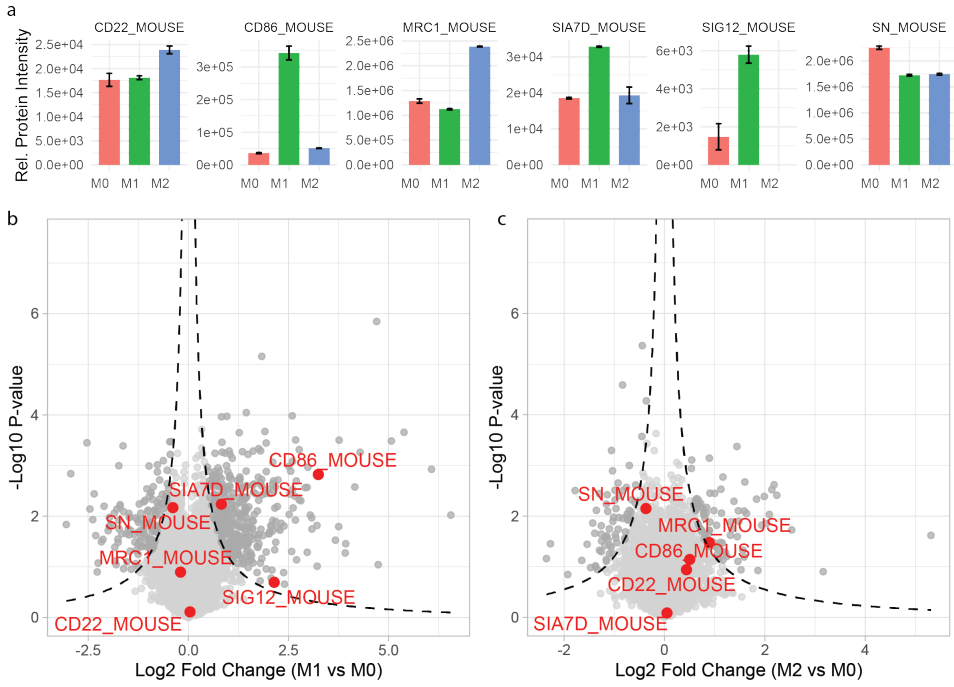

Figure 6.2: Identification of Siglecs in macrophages using whole cell LC-MS/MS proteomics. (**a**) Relative quantification of indicated proteins of interest in all three polarization states (**b**) Violin plots. Non-significant proteins are in light gray, significantly upregulated proteins in dark grey and in red are highlighted and annotated proteins. Significance was assessed using a Student's t-test. Dashed lines represent a hyperbolic cutoff ($-\log_{10}(p) > 1.3/|\log_2 \mathrm{FC}| - 0.1$), imposing stricter significance for small fold changes and more permissive thresholds for large effects.

glucose transporters are genetically removed could be employed such as Cre-LoxP conditional systems that are available for GLUT1, although artefacts based on the essential nature of this transporter may be expected.[23,24] Second, transient knock-down could be achieved using siRNA technology as in D'Souza *et al*.[25] However, a more straightforward approach might entail a competition experiment with fluorinated radioactive glucose analogs that have traditionally been used as sensors for glucose uptake *in vivo* and for which extensive kinetic profiles are known.[26] For this, the glucose analogs 2-^{18}FDG and 6-^{18}FDG would be suitable candidates (**Figure 6.3**) as they emit β^+ positrons that are detectable in whole tissues. The 2-deoxy variant is an accumulation probe because of its free 6-hydroxyl position and concomitant inhibition of glycolysis beyond hexokinase. This molecule is generally considered a true glucose sensor with high signal-to-noise ratios and is often used in clinical practice for detection of tumors and imaging of therapy response in humans.[27,28] Next to this accumulation probe, competition of our analog 6-DAG with ^{18}FDG would reveal the precise contri-

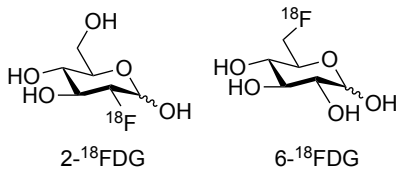

Figure 6.3: Chemical structures of fluorinated radiolabeled glucose analogs

bution of accumulation over true glucose flux. It must be noted however, that such an experiment would be most insightful when performed on the specific sorted immune subpopulations for which 6-DAG uptake was glucose-insensitive. Lastly, following the principles of standard Michaelis-Menten transporter kinetics, determination of the inhibitory constant K_i of glucose for 6-DAG, by simple calculation of the initial rate at several fixed concentrations of glucose, could provide more insight into the similarity of the two substrates. Namely, when $K_i \approx K_M$, "the operation of a simple common carrier is indicated", as is stated by Romano *et al*.[29]

An additional and largely unexplored aspect of 6-DAG concerns its intracellular retention following fixation, permeabilization, and click chemistry. As a non-reactive glucose analog lacking an obvious functional group for covalent crosslinking, it remains unclear how 6-DAG is retained within cells after paraformaldehyde fixation. This is especially intriguing given the large number of washing steps that are inherently part of click chemistry and flow cytometry staining protocols. Following chemical intuition, one would predict the highly polar conjugate between a sulfated AF647 azide fluorophore and an alkyne sugar to be extremely easily removed after repeated PBS-based washing steps. One possibility is that only a subset of 6-DAG becomes indirectly immobilized through association with proteins or membranes, for example following unknown metabolic processing or compartmentalization. In this scenario, the detected signal would reflect a specific, retained fraction of intracellular glucose rather than the total uptake pool, potentially biasing interpretation of uptake measurements. Alternatively, 6-DAG may participate in currently uncharacterized chemical interactions during fixation, or undergo partial modification that promotes retention.

These considerations are particularly relevant in light of the correlation analyses presented in **Chapter 5**, where glucose uptake appeared variably constrained by cell abundance. If only a retained subpool of 6-DAG is measured, shifts in correlation structure upon immune activation may reflect changes in intracellular processing or retention rather than uptake alone. Future work could therefore focus on dissecting the chemical basis of 6-DAG retention, for example by comparing fixation-dependent and fixation-independent detection strategies, or by designing next-generation probes with defined crosslinking capabilities similar to the ones proposed by Hamachi and coworkers.[30] Such probes could enable discrimination between freely diffusible, metaboli-

cally processed, and structurally associated glucose pools, thereby refining interpretation of nutrient uptake measurements at the single-cell level.

6.5 Methods

Statistical re-analysis of sialoside binding Statistical re-analysis was performed in R on the Glyco-PAINT-APP binding data obtained in **Chapter 4**. For all methods, the residence time (τ) derived from square-level analysis was used as the primary outcome variable. For the square-level ANOVA, data were treated as $n = 5651$ independent observations. A one-way ANOVA was performed using the `aov()` function, followed by Tukey's Honest Significant Difference (HSD) post-hoc test for pairwise comparisons between M0, M1, and M2 conditions. For the recording-level ANOVA, square-level data were first aggregated by calculating the mean of τ for each individual microscopy recording ($n = 9$ per condition). These means were then subjected to a one-way ANOVA and Tukey HSD test. For linear mixed-effects modeling (LMM), the hierarchical structure was explicitly modeled using the `lme4` package. Adjuvant condition was treated as a fixed effect, while the recording ID was included as a random intercept: $Y \sim \text{Adjuvant} + (1 \mid \text{Recording})$. Degrees of freedom were estimated using Satterthwaite's approximation via the `lmerTest` package. Pairwise comparisons of estimated marginal means (EMMs) were performed using the `emmeans` package with Tukey adjustment for multiple comparisons.

Principal Component Analysis Multivariate dimensionality reduction was performed using Principal Component Analysis (PCA) to evaluate the variance structure of the Glyco-PAINT kinetic data. A total of 12 kinetic features were extracted for each square to serve as input variables: Density (k_{on}), Average Residence Time (τ), Median Diffusion Coefficient, Median Long Track Duration, Median Short Track Duration, Total Track Duration, Total Displacement, Median Track Duration, Median Displacement, Max Displacement, Median Max Speed, and Median Mean Speed. Prior to analysis, features were Z-score normalized (centered and scaled to unit variance). PCA was calculated using the `prcomp` function in R. The contribution of each feature to the global variance was visualized via loading vectors, while adjuvant-specific clustering was evaluated by projecting individual square scores onto the first two principal components (PC1 and PC2).

Sample preparation using suspension-trapping (S-Trap) Protein lysates were prepared in lysis buffer containing 5% (w/v) sodium dodecyl sulfate (SDS; Sigma-Aldrich, L6026) and 50 mM triethylammonium bicarbonate (TEAB; Sigma-Aldrich, T7408), pH 8.5. Samples were homogenized by vortexing and, when necessary, sonicated to reduce DNA-induced viscosity. Protein concentration was determined by BCA assay (Thermo Fisher Scientific), ensuring that BSA standards were diluted in the same lysis buffer to correct for SDS interference. A total of 10 µg protein in a final volume of 50 µL was used per sample. Proteins were reduced with 5 mM dithiothreitol (DTT; Sigma-Aldrich, R0862) for 15 min at 65 °C and cooled to room

temperature, followed by acidification to 1.1% (v/v) phosphoric acid (Sigma-Aldrich, 49685). To precipitate proteins and enable suspension trapping, 400 µL of S-Trap binding buffer was added; this buffer consisted of 90% (v/v) LC-MS grade methanol (Biosolve, 136841) and 100 mM TEAB (from a 1 M TEAB stock, pH adjusted to 7.5 with phosphoric acid and diluted 1:10). The entire sample was loaded onto S-Trap microcolumns (Zymo-Spin I Columns, Zymo Research, C1003) and centrifuged at 1,400 *g* for 1–2 min to trap proteins. Columns were washed three times with 400 µL binding buffer and once with 400 µL 90% (v/v) methanol to remove residual detergent and salts.

On-column digestion was performed by adding 50 µL of 50 mM ammonium bicarbonate (ABC; Sigma-Aldrich, 09830) containing sequencing-grade trypsin (Promega, V5111) at a 1:10 (w/w) enzyme-to-protein ratio, with a minimum of 0.1 µg trypsin per sample. Digestion proceeded overnight at 37 °C. Peptides were sequentially eluted by centrifugation with: (i) 50 mM ABC, (ii) 0.1% (v/v) formic acid (FA; Biosolve, 069141) in LC-MS grade water (Biosolve, 232141), and (iii) 60% (v/v) acetonitrile (ACN; Biosolve, 012078) with 0.1% FA. Combined eluates were dried under vacuum and resuspended in 0.1% FA. Samples were desalted using StageTips prepared according to Rappsilber *et al*[31], dried, and stored at −20 °C before LC–MS/MS analysis.

LC–MS/MS Data Acquisition and DIA-NN Processing Peptides were analyzed on a timsTOF Pro mass spectrometer (Bruker Daltonics) coupled to a nanoElute UHPLC system (Bruker). Approximately 200 ng of peptide was loaded onto a C18 analytical column and separated using a 60 min linear gradient from 2% to 35% ACN in 0.1% FA at 300 nL/min. Data were acquired in diaPASEF mode with ion mobility separation over a $1/k_0$ range of 0.6–1.6 V·s/cm^2. DIA windows were automatically optimized across the mobility dimension. Raw files were processed using DIA-NN (version 2.0) in library-free mode with deep-learning spectral prediction and retention time profiling enabled.[32] Protein inference was performed using gene-level grouping, and protein intensities were exported as normalized quantitative values for downstream statistical analysis in R.

References

(1) Lelek, M.; Gyparaki, M. T.; Beliu, G.; Schueder, F.; Griffié, J.; Manley, S.; Jungmann, R.; Sauer, M.; Lakadamyali, M.; Zimmer, C. Single-molecule localization microscopy. *Nature Reviews Methods Primers* **2021**, *1*, 39.

(2) Riera, R.; Hogervorst, T. P.; Doelman, W.; Ni, Y.; Pujals, S.; Bolli, E.; Codée, J. D. C.; van Kasteren, S. I.; Albertazzi, L. Single-molecule imaging of glycan–lectin interactions on cells with Glyco-PAINT. *Nature Chemical Biology* **2021**, *17*, 1281–1288.

(3) Tholen, M. M.; Riera, R.; Izquierdo-Lozano, C.; Albertazzi, L. Multiplexed Lectin-PAINT super-resolution microscopy enables cell glycotyping. *Communications biology* **2025**, *8*, 267.

REFERENCES

(4) E. Tholen, M. M.; P. Tas, R.; Wang, Y.; Albertazzi, L. Beyond DNA: new probes for PAINT super-resolution microscopy. *Chemical Communications* **2023**, *59*, 8332–8342.

(5) Albertazzi, L.; Heilemann, M. When Weak Is Strong: A Plea for Low-Affinity Binders for Optical Microscopy. *Angewandte Chemie International Edition* **2023**, *62*, e202303390.

(6) Ha, T.; Tinnefeld, P. Photophysics of Fluorescent Probes for Single-Molecule Biophysics and Super-Resolution Imaging. *Annual Review of Physical Chemistry* **2012**, *63*, 595–617.

(7) Dempsey, G. T.; Vaughan, J. C.; Chen, K. H.; Bates, M.; Zhuang, X. Evaluation of fluorophores for optimal performance in localization-based super-resolution imaging. *Nature Methods* **2011**, *8*, 1027–1036.

(8) Jungmann, R.; Avendaño, M. S.; Woehrstein, J. B.; Dai, M.; Shih, W. M.; Yin, P. Multiplexed 3D cellular super-resolution imaging with DNA-PAINT and Exchange-PAINT. *Nature methods* **2014**, *11*, 313–318.

(9) Kozak, M.; Piepho, H.-P. What's normal anyway? Residual plots are more telling than significance tests when checking ANOVA assumptions. *Journal of Agronomy and Crop Science* **2018**, *204*, 86–98.

(10) Schank, J. C.; Koehnle, T. J. Pseudoreplication is a pseudoproblem. *Journal of Comparative Psychology* **2009**, *123*, 421–433.

(11) Colegrave, N.; Ruxton, G. D. Using Biological Insight and Pragmatism When Thinking about Pseudoreplication. *Trends in Ecology & Evolution* **2018**, *33*, 28–35.

(12) Daniel, W. W.; Cross, C. L., *Biostatistics: A Foundation for Analysis in the Health Sciences*; John Wiley & Sons: 2018.

(13) Kuznetsova, A.; Brockhoff, P. B.; Christensen, R. H. B. lmerTest Package: Tests in Linear Mixed Effects Models. *Journal of Statistical Software* **2017**, *82*, 1–26.

(14) Carnoli, A. J.; Lohuis, P. O.; Buydens, L. M. C.; Tinnevelt, G. H.; Jansen, J. J. Linear Mixed-Effects Models in chemistry: A tutorial. *Analytica Chimica Acta* **2024**, *1304*, 342444.

(15) Segura, E.; Albiston, A. L.; Wicks, I. P.; Chai, S. Y.; Villadangos, J. A. Different cross-presentation pathways in steady-state and inflammatory dendritic cells. *Proceedings of the National Academy of Sciences* **2009**, *106*, 20377–20381.

(16) Segura, E.; Gupta, N.; Albiston, A. L.; Wicks, I. P.; Chai, S. Y.; Villadangos, J. A. Reply to Burgdorf et al.: The mannose receptor is not involved in antigen cross-presentation by steady-state dendritic cells. *Proceedings of the National Academy of Sciences* **2010**, *107*.

(17) Burgdorf, S.; Kautz, A.; Böhnert, V.; Knolle, P. A.; Kurts, C. Distinct Pathways of Antigen Uptake and Intracellular Routing in CD4 and CD8 T Cell Activation. *Science* **2007**, *316*, 612–616.

(18) Burgdorf, S.; Schuette, V.; Semmling, V.; Hochheiser, K.; Lukacs-Kornek, V.; Knolle, P. A.; Kurts, C. Steady-state cross-presentation of OVA is mannose receptor-dependent but inhibitable by collagen fragments. *Proceedings of the National Academy of Sciences* **2010**, *107*.

(19) Rauen, J.; Kreer, C.; Paillard, A.; van Duikeren, S.; Benckhuijsen, W. E.; Camps, M. G.; Valentijn, A. R. P. M.; Ossendorp, F.; Drijfhout, J. W.; Arens, R.; Burgdorf, S. Enhanced Cross-Presentation and Improved CD8+ T Cell Responses after Mannosylation of Synthetic Long Peptides in Mice. *PLoS ONE* **2014**, *9*, ed. by Kassiotis, G., e103755.

(20) Alam, S.; Davies, G.; Lin, C. M.; Zal, T.; Nasholds, W.; Jameson, S. C.; Hogquist, K. A.; Gascoigne, N. R.; Travers, P. J. Qualitative and Quantitative Differences in T Cell Receptor Binding of Agonist and Antagonist Ligands. *Immunity* **1999**, *10*, 227–237.

(21) Dual actions of group B Streptococcus capsular sialic acid provide resistance to platelet-mediated antimicrobial killing | PNAS.

(22) Tsuchiya, M.; Tachibana, N.; Hamachi, I. Post-click labeling enables highly accurate single cell analyses of glucose uptake ex vivo and in vivo. *Communications Biology* **2024**, *7*, 459.

(23) Freemerman, A. J. et al. Myeloid Slc2a1-Deficient Murine Model Revealed Macrophage Activation and Metabolic Phenotype Are Fueled by GLUT1. *The Journal of Immunology Author Choice* **2019**, *202*, 1265–1286.

(24) Pereverzeva, L.; Léopold, V.; Saris, A.; Schuurman, A. R.; Butler, J. M.; Reijnders, T. D. Y.; Roelofs, J. J. T. H.; Faber, D. R.; Wiersinga, W. J.; van't Veer, C.; de Vos, A. F.; van der Poll, T. Role of Myeloid Cell Glucose Transporter 1 in the Host Response During Pneumonia Caused by Streptococcus pneumoniae. *International Journal of Molecular Sciences* **2025**, *26*, 10461.

(25) D'Souza, L. J.; Wright, S. H.; Bhattacharya, D. Genetic evidence that uptake of the fluorescent analog 2NBDG occurs independently of known glucose transporters. *PLOS ONE* **2022**, *17*, ed. by Fujii, H., e0261801.

(26) Campbell, E.; Jordan, C.; Gilmour, R. Fluorinated carbohydrates for 18F-positron emission tomography (PET). *Chemical Society Reviews* **2023**, *52*, 3599–3626.

(27) Wong, A. N. M.; McArthur, G. A.; Hofman, M. S.; Hicks, R. J. The Advantages and Challenges of Using FDG PET/CT for Response Assessment in Melanoma in the Era of Targeted Agents and Immunotherapy. *European Journal of Nuclear Medicine and Molecular Imaging* **2017**, *44*, 67–77.

(28) Muzic, R. F.; Chandramouli, V.; Huang, H.-M.; Wu, C.; Wang, Y.; Ismail-Beigi, F. Analysis of Metabolism of 6FDG: A PET Glucose Transport Tracer. *Nuclear medicine and biology* **2011**, *38*, 667–674.

(29) Romano, A. H.; Connell, N. D. 6-deoxy-D-glucose and D-xylose: analogs for the study of D-glucose transport by mouse 3T3 cells. *Journal of Cellular Physiology* **1982**, *111*, 77–82.

(30) Nonaka, H.; Mino, T.; Sakamoto, S.; Oh, J. H.; Watanabe, Y.; Ishikawa, M.; Tsushima, A.; Amaike, K.; Kiyonaka, S.; Tamura, T.; Radu Aricescu, A.; Kakegawa, W.; Miura, E.; Yuzaki, M.; Hamachi, I. Revisiting PFA-mediated tissue fixation chemistry: *FixEL* enables trapping of small molecules in the brain to visualize their distribution changes. *Chem* **2023**, *9*, 523–540.

(31) Rappsilber, J.; Mann, M.; Ishihama, Y. Protocol for micro-purification, enrichment, pre-fractionation and storage of peptides for proteomics using StageTips. *Nature Protocols* **2007**, *2*, 1896–1906.

(32) Demichev, V.; Messner, C. B.; Vernardis, S. I.; Lilley, K. S.; Ralser, M. DIA-NN: neural networks and interference correction enable deep proteome coverage in high throughput. *Nature Methods* **2020**, *17*, 41–44.